ELSEVIER

Environmental Modelling & Software 13 (1998) 247–255

Environmental
Modelling & Software

A numerical method for two-phase flows with an interface

Li Chen *, Yuguo Li

Advanced Fluids Dynamics Laboratory, CSIRO Building, Construction and Engineering, Highett, Victoria 3190, Australia

Abstract

One of the challenges in modelling multiphase fluid systems is to capture accurately the discontinuous-interface phenomenon. In this paper a numerical model for two-phase flows with a varying density is presented, in which a modified volume of fluid (VOF) method is combined with a semi-implicit algorithm (SIMPLE) and a higher-order advection scheme in a collocated grid. The improved volume tracking method allows interfaces to be captured and maintained compactly in one cell, without imposing restrictions on the topological complexity or the number of interfaces that can be represented. The surface tension force is modelled by a continuum surface force approximation. An efficient solver is used for the resulting system of the linear equations. Example problems simulated in this paper are the buoyancy-driven motion of multiple bubbles in a viscous liquid, and bubble-rise towards an interface. The complex topological changes that occur during bubble rise are well predicted. The result is verified by experimental data in the literature.

Keywords: Bubble coalescence; Bubble deformation; Convection scheme; Interface fragmentation; Interface tracking; Two-phase flow; Volume of fluid (VOF) method

1. Introduction

Flows with a spatial variation of fluid properties, such as gas–liquid interfaces due to density variation, can be found in many engineering and environmental applications. The generation of vorticity by the interaction of non-parallel pressure and discontinuous fluid properties produces a complex flow structure and scale, which presents a computational challenge. A robust algorithm for solving multi-phase flows with an accurate representation of interfaces is required to accommodate the complex topological changes.

Conventional algorithms for the solution of flows with an interface are associated with an explicit scheme for momentum advection on a staggered grid (e.g. Lafaurie et al., 1994; Unverdi and Tryggvason, 1992). The use of an explicit scheme reduces the computational efficiency owing to the limitations of the Courant-Friedrichs-Lew (CFL) condition. At the same time, staggered grids present some difficulties for three-dimensional flows with complex geometry. Recently, a second-order time-accurate algorithm based on the Godunov technique has been developed to simulate such a flow by Rider et al. (1995). In their projection algorithms, the convection terms are explicitly discretized with a second-order upwind scheme in a flux-limited fashion.

Regarding interface tracking techniques, the boundary integral (Ryskin and Leal, 1984) and Lagrangian finite element (Unverdi and Tryggvason, 1992) methods are able to simulate flows with interfaces, but it may be difficult for them to handle the fragmentation and coalescence of complex interfacial phenomena. The marker and cell (MAC) and volume tracking techniques (volume of fluid: (VOF)) due to Hirt and Nichols (1982) remain quite effective. In the conventional MAC method, the interface is represented by Lagrangian marker particles advected by the local velocity. As a result, it can not accurately define an interface, especially for three-dimensional flow, nor properly conserve mass. However, one favoured feature of this method is that, unlike any other, no numerical diffusion exists. Therefore, some improvement to this method can still be promising (Rider et al., 1995).

In this paper, an improvement to the method of Chen et al. (1996, 1997) is presented. It models multi-phase flows with complex interfacial phenomena on collocated grids. The method is conservative for both mass and

* Corresponding author.

1364-8152/98/$—see front matter
PII: S1364-8152(98)00025-5

momentum. A semi-implicit scheme for the velocity equations is used. The velocity–pressure coupling is based on SIMPLE.

2. Mathematical formulation

The governing equation for a multiphase flow with a density varying interface is given by the Navier–Stokes equation, which can be written in a non-dimensional form as

$$\nabla \cdot \mathbf{U} = 0, \tag{1}$$

$$\frac{\partial(\rho \mathrm{U})}{\partial t} + \nabla \cdot (\rho \mathbf{U} \otimes \mathbf{U}) = -\nabla p + \rho \mathbf{g} + \frac{1}{\mathrm{Re}} \nabla \cdot [\mu(\nabla \mathbf{U} + \nabla \mathbf{U}^{\mathrm{T}})] + \frac{1}{\mathrm{Bo}} \mathbf{F}_{sv}, \tag{2}$$

with scales

$$p^* = \frac{p}{p_{ref}}, \mathbf{U}^* = \frac{\mathbf{U}}{u_{ref}}, \mathbf{x}^* = \frac{\mathbf{x}}{R_0}, \tau = \frac{t}{t_{ref}} \tag{3}$$

$$\rho^* = \frac{\rho}{\rho_{ref}}, \mu^* = \frac{\mu}{\mu_{ref}}, \sigma^* = \frac{\sigma}{\sigma_{ref}}.$$

Here

$$u_{ref} = \sqrt{gR_0}, p_{ref} = \rho_{ref} u_{ref}^2. \tag{4}$$

Note that * is omitted in Eqs. (1) and (2) for convenience. The inner product of tensors is denoted by $\otimes$, $\mathbf{U}(u_r,u_\theta,u_z)$ is the fluid velocity in $\mathbf{x}(r,\theta,z)$ and $\boldsymbol{F}_{sv}$ the volume form of the surface tension force. ρ is the density, μ the dynamic viscosity, p the pressure, $\mathbf{g}(0,0,g)$ the gravity vector, R_0 initial bubble radius, and σ the surface tension coefficient. The subscript, *ref*, stands for reference value. Here, liquid properties are adopted as reference values. Reynolds and Bond numbers are defined by

$$\mathrm{Re} = \frac{\rho_f g^{1/2} R_0^{3/2}}{\mu_{ref}}, \; Bo = \frac{\rho_f g R_0^2}{\sigma},$$

and the properties of a fluid are given by

$$\rho(\mathbf{x},t) = F(\mathbf{x},t)\rho_f + [1 - F(\mathbf{x},t)]\rho_g, \tag{5}$$

$$\mu(\mathbf{x},t) = F(\mathbf{x},t)\mu_f + [1 - F(\mathbf{x},t)]\mu_g. \tag{6}$$

Here F is the local volume fraction of one fluid. Its value may be unity in the liquid phase and zero in the gas phase if a gas–liquid two-phase system is involved. A value between 1 and 0 indicates a density interface. The subscripts, f and g, indicate liquid and gas phases, respectively. The last term in Eq. (2), $\boldsymbol{F}_{sv}$, is modelled using the continuum surface force (CSF) model developed by Brackbill et al. (1992). In this model, an interface is interpolated as a transient region with a finite thickness. Thus the surface tension force localized in this region is converted into a volume force with the help of a Dirac delta function concentrated on the surface. The surface tension force is written as

$$\mathbf{F}_{sv} = \sigma \kappa(\mathbf{x}) \frac{\nabla \tilde{c}(\mathbf{x})}{[\tilde{c}]}, \tag{7}$$

The curvature is given by

$$\kappa = -(\nabla \cdot \mathbf{n}), \tag{8}$$

and a unit normal vector to a surface is defined by

$$\mathbf{n} = \frac{\nabla \tilde{c}}{|\nabla \tilde{c}|}. \tag{9}$$

Here $\tilde{c}$ in the above equations is a colour function and $[\tilde{c}]$ is the difference in the value of the colour function between two phases. Instead of using it directly, Eq. (8) can be expanded in terms of the normal vector to a surface, $\mathbf{n}$, as

$$\kappa = \frac{1}{|\mathbf{n}|}\left[\left(\frac{\mathbf{n}}{|\mathbf{n}|} \cdot \nabla\right)|\mathbf{n}| - (\nabla \cdot \mathbf{n})\right] \tag{10}$$

Eq. (10) seems to produce a better calculation of surface tension because it uses a wider stencil than Eq. (8).

The problem of a flow with a varying density is fully defined when a governing equation for a dynamic interface is given. It is noted that Eqs. (5) and (6) represent discontinuous properties of a multiphase fluid, which implies an interface, and they can be used to monitor the dynamics of the interface. However, when a large discontinuity is involved, for example a discontinuity of 850 in density ratio exists for a water–air system, numerical difficulties may arise in identifying an 'exact' interface and defining the fluid properties. Thus, instead of solving the density transport equation directly, the volume fraction of liquid, F, is used to identify an interface. The transport of this function is given by

$$\frac{\partial F}{\partial t} + \nabla \cdot (\mathbf{U}F) = 0 \tag{11}$$

Also, the colour function in Eqs. (7) and (9) can be replaced by the function F.

Now a problem can be specified with suitable initial and boundary conditions and solved numerically with an appropriate method.

3. Numerical method

A control volume technique is used to discretize the PDEs. The computational domain is divided into a number of non-overlapping control volumes and all variables are defined at the centre of the control volume. Such a collocated arrangement of the grid may reduce the accuracy of the diffusive term, but it has advantages, such as an accurate representation of flux and source terms. The collocated grid is illustrated in Fig. 1. The differential equations are integrated over each control volume. For any variable, ϕ, the time integral over a control volume P of a size, ΔV_P, is given by

$$\int_{\Delta V}\left(\frac{\partial\phi}{\partial\tau}\right)dV = \frac{\phi^{n+1}_{i,j,k} - \phi^{n}_{i,j,k}}{\Delta\tau}\,\Delta V_P \tag{12}$$

For the orthogonal grid used in this study, convection and diffusion terms are written after integration as

$$\int_{\Delta V}[\nabla\cdot(G\phi) - \nabla\cdot(\Gamma\nabla\phi)]dV = (J^D + J^C)_e - (J^D + J^C)_w + (J^D + J^C)_n - (J^D + J^C)_s + (J^D + J^C)_t - (J^D + J^C)_b. \tag{13}$$

For example, the diffusion contribution at the east face of the control volume P, J^D_e, is linearized by central differencing as

$$J^D_e = -\left(\Gamma\frac{\partial\phi}{\partial x}A\right)_e = -\frac{[\alpha_{2e}\Gamma_E + (1-\alpha_{2e})\Gamma_P]}{0.5(\Delta x_P + \Delta x_E)}(\phi_E - \phi_P)A_e \tag{14}$$

The linearizations of the diffusion terms on other faces are similar. It should be noted that the accuracy of a solution may be reduced if $\Delta x_P \neq \Delta x_E$ in Eq. (14). The convection contribution is given by generalized form with the well-known deferred correction expression as

$$J^C_e = G^+_e\phi_P + G^-_e\phi_E + (G\phi)^{dc}_e \tag{15}$$

in which, the first-order upwind mass flux is defined by

$$G^+_e = \frac{G_e + |G_e|}{2},\quad G^-_e = \frac{G_e - |G_e|}{2} \tag{16}$$

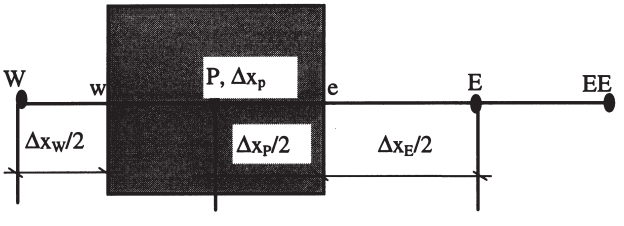

Fig. 1. Schematic arrangement of a grid system in the x-direction.

and

$$(G\phi)^{dc}_e = [\alpha_{1e}\phi_E + (\alpha_{2e}-1)\phi_P - q_e(\phi_E - \beta_{2e}\phi_P + \beta_{1e}\phi_W)]G^+_e + [(\alpha_{2e}-1)\phi_E + \alpha_{1e}\phi_P - q_e(\phi_P - \beta_{2e}\phi_E + \beta_{1e}\phi_{EE}))G^-_e \tag{17}$$

For a uniform grid, the geometric parameters are equal to $\alpha_{1e} = 0.5$, $\alpha_{2e} = 0.5$, $\beta_{1e} = 1$ and $\beta_{2e} = 2$, respectively. By varying the deferred correction term, a higher order scheme for the convection term can be obtained (see Li (1997) for details). For a uniform grid, in the second-order central differencing (CD), $q_e = 0$; q_e is equal to 1/8 or 1/6 for a second- or third-order accurate QUICK scheme, respectively, and equal to $\max\{0.0.5 - 1/|Pe_e|\}$ for the second-order HYBRID scheme (SHYBRID). The definition of local Peclet number, Pe_e, is calculated by $0.5G_e(\Delta x_P + \Delta x_E)/(\Gamma_e A_e)$. The flux G_e is calculated by Rhie–Chow's interpolation technique. This technique effectively overcomes the difficulty of the decoupling between pressure and velocity raised by a linear interpolation and guarantees a global mass conservation.

As the grid point is always located at the centre of a control volume, a representative source is obtained by

$$\int_{\Delta V} sdV = s_P\Delta V_P \tag{18}$$

The surface tension force is linearized by a 27-point stencil for a three-dimensional surface. The detail of an implementation can be found in Chen et al. (1996).

To capture the sophisticated dynamics of an interface,

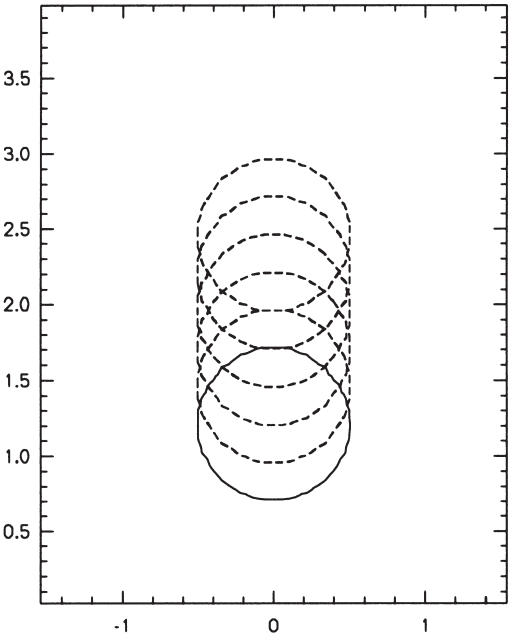

Fig. 2. Translation of a spherical blob with a constant velocity using the modified VOF method. ($\Delta z = \Delta r = 0.04$, $\Delta t = 0.01$, 300 iterations).

an accurate technique is needed to solve Eq. (11). In this study, a modified line constant VOF method is used (see Chen et al., 1996). In this method, the interface tracking is divided into three steps: (1) reconstruction of the surface based on the calculated unit normal to the surface, which is required in the surface tension calculation; (2) to advection of the surface by the local velocity using first-order upwind or downwind schemes; (3) ensuring the value of each local volume fraction F does not exceed the range 0 to 1. The upwind scheme is numerically diffusive; and a downwind scheme has the advantage of maintaining the sharpness of a surface, but it is numerically unstable. In the original VOF method, a surface can only be considered as either parallel or perpendicular to the flux direction, thus the numerical diffusion is unavoidable in some flow situations, such as when a surface has a 45° angle to the velocity field. In our modified VOF, the upwind and downwind schemes are combined based on the surface orientation to achieve an accurate advection of a surface. When a surface is considered parallel to the flux direction, the upwind scheme is used, otherwise the downwind scheme is used. The definition of parallel or perpendicular to the flux direction is determined by the respective component of the unit normal to a surface, $\mathbf{n}(n_r,n_\theta,n_z)$, in Eq. (9). It can be adjusted on the basis of the velocity field. Due to adopting a constant line structure for a surface, special care is required to restrict an over- or under-flux when the downwind scheme is used. The implementation details can be found in Lafaurie et al. (1994). It is believed that a slope-line VOF method, e.g. Youngs' method (Youngs, 1982), overcomes such an over- or under-flux problem and is able to produce a better result. Youngs' method has not been implemented here.

To demonstrate our front tracking method, a test problem of a spherical 'blob' axisymmetrically rising in a liquid with a constant velocity field $\mathbf{U}\{u_r,u_z\} = \{0,0.5\}$ was performed in which the upwind scheme was used

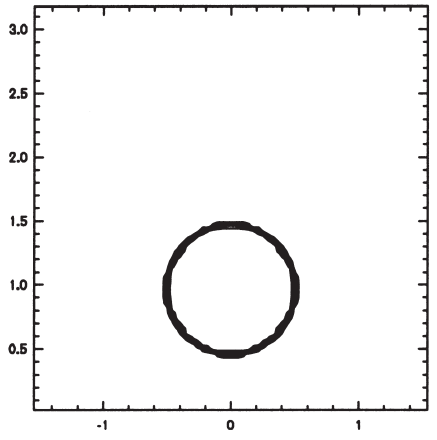

(a) Initial Condition

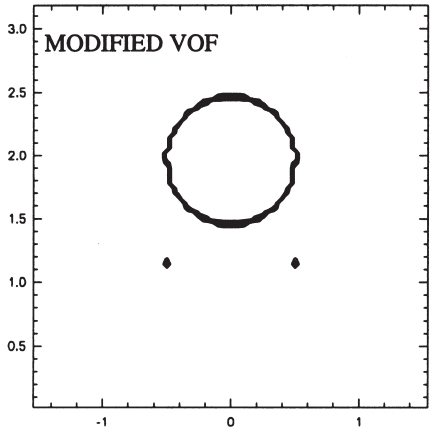

(b) at 200th steps

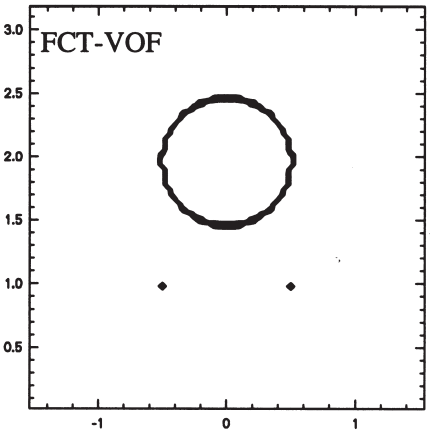

(c) at 200th steps

Fig. 3. Comparison between present VOF and FCT–VOF for a sphere rising at a constant velocity $\Delta r = \Delta z = 0.04$, $\Delta t = 0.01$.

when the unit normal component was less than 0.3. This means that the upwind scheme switches to the downwind scheme whenever the angle between a surface and a flux direction is greater than 17.3°. The motion of the blob is shown in Fig. 2 and a very well conserved volume and shape of the spherical 'blob' is obtained. The present method was compared with a flux-correct-technique (FCT)–VOF scheme due to Zalesak (1979) for the spherical blob problem at the 200th time step. In the FCT–VOF method, the diffusive scheme was a first-order upwind scheme and a downwind scheme was used for an anti-diffusive flux to correct the diffusion resulting from the upwind scheme. The result is shown in Fig. 3. It can be seen that good agreement between the two schemes is obtained. This may be due to the fact that both schemes use the same anti-diffusion scheme (downwind scheme) so that they have the same order of accuracy. However, the simplicity in implementation and flexibility in coupling with the flow field may be advantages of the present method. A higher-order anti-diffusive flux can improve the accuracy of the FCT method and will be the subject of future research.

A semi-implicit scheme is used to solve Eq. (2) for the velocity field and the SIMPLE method is adopted for the velocity–pressure coupling. The resultant non-symmetrical system arising from the momentum equation is solved by the SIP or bi-conjugate gradient method with incomplete Cholesky preconditioning. The symmetric system due to pressure correction is solved by the conjugate gradient method with incomplete Cholesky preconditioning.

Two test problems, bubble coalescence and rise towards a free surface, are simulated by the present model. Before the simulations, a grid-independent test was carried out on the axisymmetric rise of a single bubble in a liquid. The bottom position of the bubble as a function of time is illustrated in Fig. 4 with three different meshes (N_z by N_r): 54 by 17, 108 by 34 and 216 by 68, which corresponds to 145, 578 and 2312 grid points in the rectangle containing the hemisphere region. It can be seen that meshes 108 by 34 seem to produce a nearly grid-independent solution. This grid size will be used in the following runs.

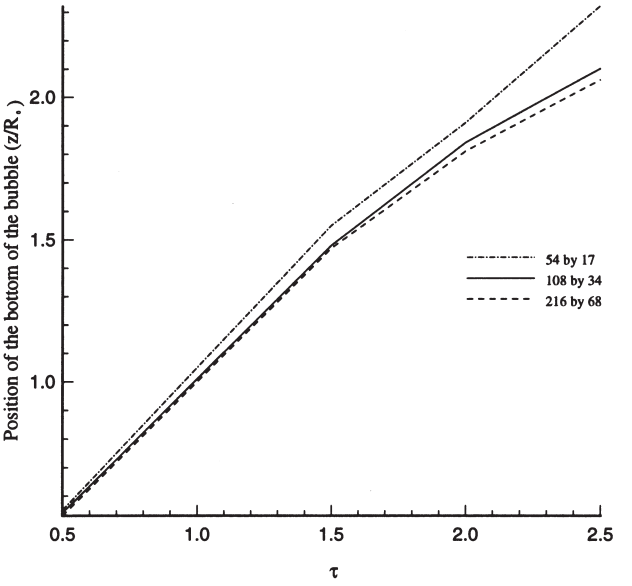

Fig. 4. Effect of grid size on the position of a bubble rising in a cylinder. (Bo = 50, Re = 100, $\rho_f/\rho_g = 80$, $\mu_f/\mu_g = 80$).

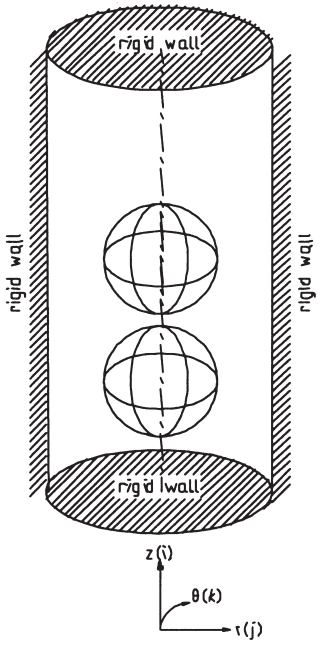

Fig. 5. Schematic description of bubble coalescence.

4. Bubble coalescence

Consider two spherical gas bubbles, referred to as leading and following bubbles, rising through a viscous liquid (see Fig. 5). The spherical gas bubbles are initially located on the axis of a vertical cylinder filled with a stationary liquid. The boundary conditions are $\mathbf{U} = 0$ at the walls. The coalescence of the two bubbles may occur while they are rising.

In general, when a single bubble rises due to the buoyancy force, the pressure gradient at the lower surface of the bubble is higher than that at the top surface of the bubble, and the vortex sheet developing at the surface has a sense of rotation, which induces a tongue of liquid jet that pushes into the bubble from below. Deformations of the bubble occur. This phenomenon was reported by a few experimentalists, e.g. Walters and Davidson (1963). For multiple bubbles, similar behaviour is expected, but the deformation and fragmentation of surfaces are more complex. Therefore the use of a higher-order convection scheme is necessary to catch the liquid jet accurately. The effect of the convection scheme was

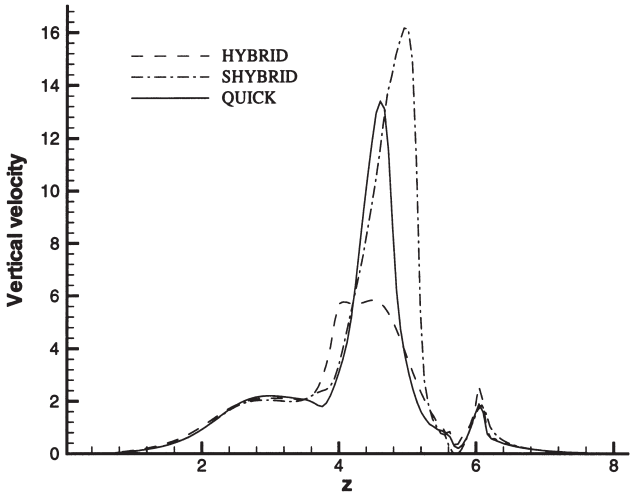

Fig. 6. Vertical velocity profile along *z*-axis with different convection schemes.

studied. As may be expected, for bubble rise with a low Reynolds number, Re = 10, the SHYBRID scheme produces the same results as HYBRID because most of the grid Peclet numbers are less than 2 and, effectively, central differencing is used in both schemes. However, with a higher Reynolds number, Re = 100, the differences between different schemes are clear, as may be seen in Fig. 6. The HYBRID scheme under-predicts the jet and a smeared solution of the velocity field is obtained. The SHYBRID scheme over-predicts the jet. The third-order QUICK scheme seems to predict the resolution of the liquid jet in terms of both its maximum value and location well. Therefore QUICK is used in the following studies.

The three-dimensional plot of the axisymmetrical coalescence of two bubbles is shown in Fig. 7. From this figure, the motion of the leading bubble induces a deformation in the following bubble, giving it a pear-like shape (Fig. 7(a,b)). Once two bubbles are approaching (Fig. 7(b)), an acceleration of the following bubble is obtained due to the low-pressure region behind the leading bubble. As time progresses, the two bubbles start to touch, as may be seen in Fig. 7(c), leaving a mushroom-like structure. Then a further fragmentation occurs and a larger spherical cap is obtained, as may be seen in Fig. 7(d).

The details of the coalescence of the two bubbles are shown in Fig. 8 for the velocity field and three contour lines of function *F*: 0.1, 0.5 and 0.9. It can be seen that the liquid circulation around each bubble produces a jet that pushes the lower surface of both leading and following bubbles, and deformations of the bubbles occur (Fig. 8(a)). Due to the effect of the velocity field around the leading bubble, the following bubble is stretched and a spherical-cap-shaped leading bubble is observed (Fig. 8(b)). After the coalescence occurs, the lower surface of the merged bubble is accelerated by the liquid jet and surface tension force and a larger spherical cap is obtained (Fig. 9(c,d)). The contour lines of *F* in Fig. 8

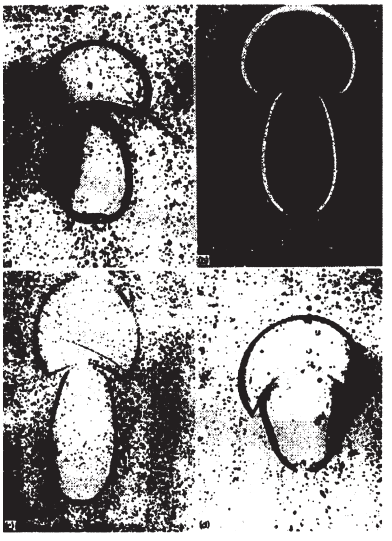

Fig. 8. Experimental result of the coalescence of two air bubbles in glycerin liquid by Narayanan et al. (1974).

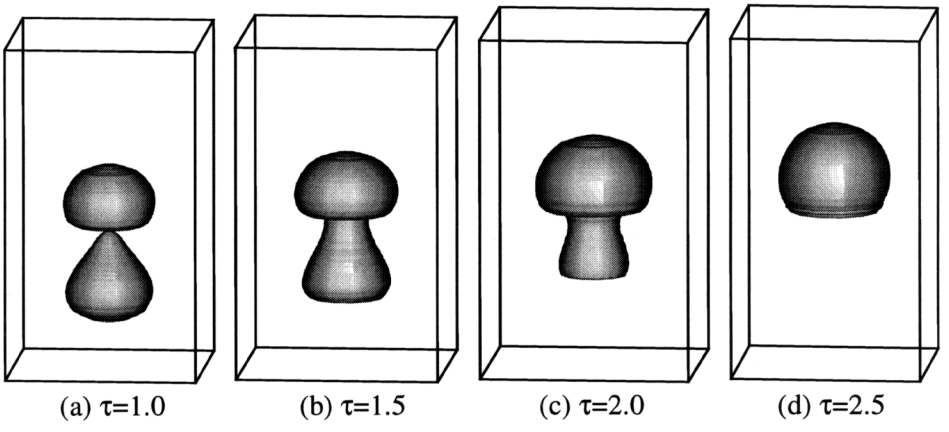

Fig. 7. Predicted the axisymmetric coalescence of two bubbles in a very viscous liquid. (Re = 10, Bo = 50, ρ_f/ρ_g = 850, μ_f/μ_g = 100, z/R_0 = 0.36).

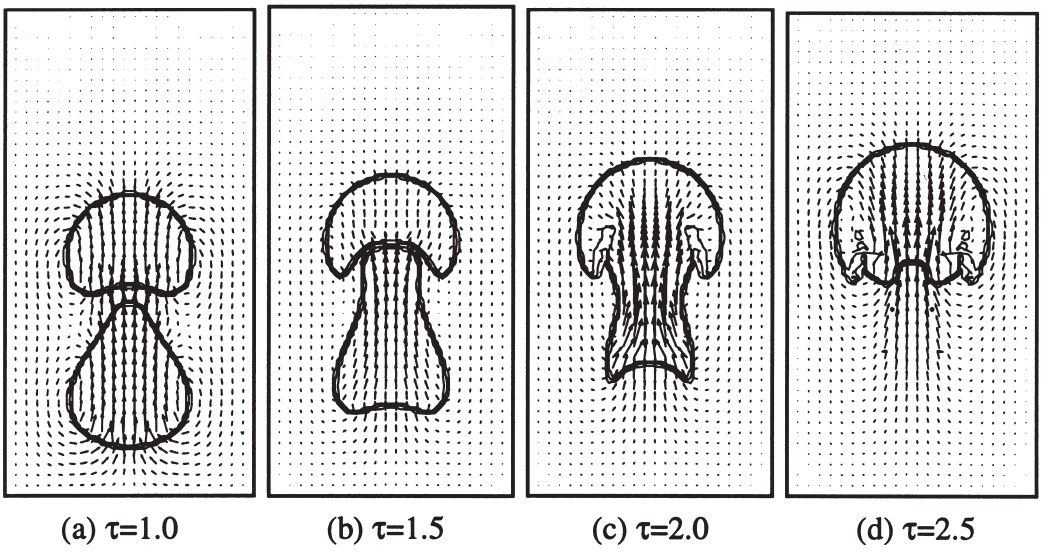

Fig. 9. Velocity field and three contours of F of the values of 0.1, 0.5 and 0.9 for the simulation in Fig. 7.

have shown an accurate representation of the bubbles with minimum numerical diffusion.

A preliminary comparison was performed between the predicted results and the experimental observations of Narayanan et al. (1974) (Fig. 2 in this reference). The similarity of the shape development of the two bubbles in the highly viscous liquid can be clearly seen from Figs. 8 and 9. Because of a lack of detail in the experiment, no quantitative comparison is possible.

5. Bubble rise towards an interface

Another test problem is a bubble rising towards a gas–liquid interface, which is also an important phenomenon occurring in many industrial and environmental applications. A schematic diagram of the problem modelled is given in Fig. 10. A bubble rises to an initially flat gas–liquid interface. The problem was simulated with Re = 30, Bo = 10, $\rho_f/\rho_g = 100$, $\mu_f/\mu_g = 100$. A low density ratio is used here for computational efficiency without losing the physics.

The simulation is shown in Fig. 11 with the plot of velocity vectors and three contours of F with the values of 0.1, 0.5 and 0.9. It can been seen that the bubble deforms during its rise and an elliptical bubble is obtained due to the viscous stress and surface tension force. The free surface is slightly deformed because of the influence of the velocity field resulting from the bubble rise (Fig. 11(b)). As time progresses, the gas–liquid interface is raised in the centre and lowered near the container walls and bubble is severely distorted by the increase in the surface tension force (Fig. 11(c, d and e)). Unlike the bubble coalescence, the vertical component of the velocity at the top of the bubble is small and the vortex around the bubble becomes strong, which

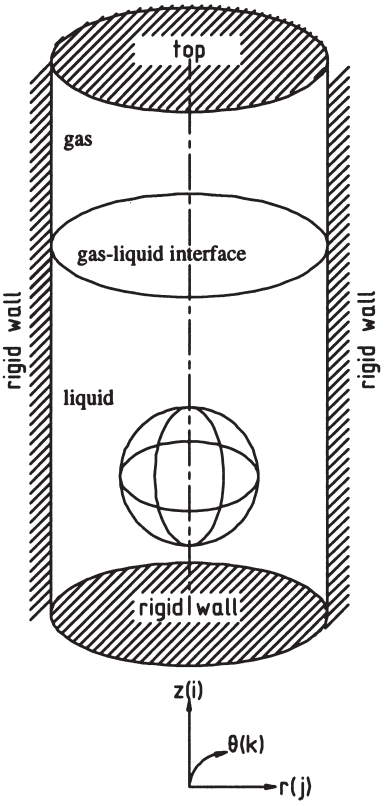

Fig. 10. A Schematic description of bubble rise towards to an interface.

stretches the bubble and interface. When the bubble approaches the interface further, the vertical velocity decreases (Fig. 11(d, e and f)) and the liquid in the thin film is pushed out mainly in the radius direction. A more flat ellipsoid is obtained (Fig. 11(e and f)).

The well-behaved contours are again indicating both

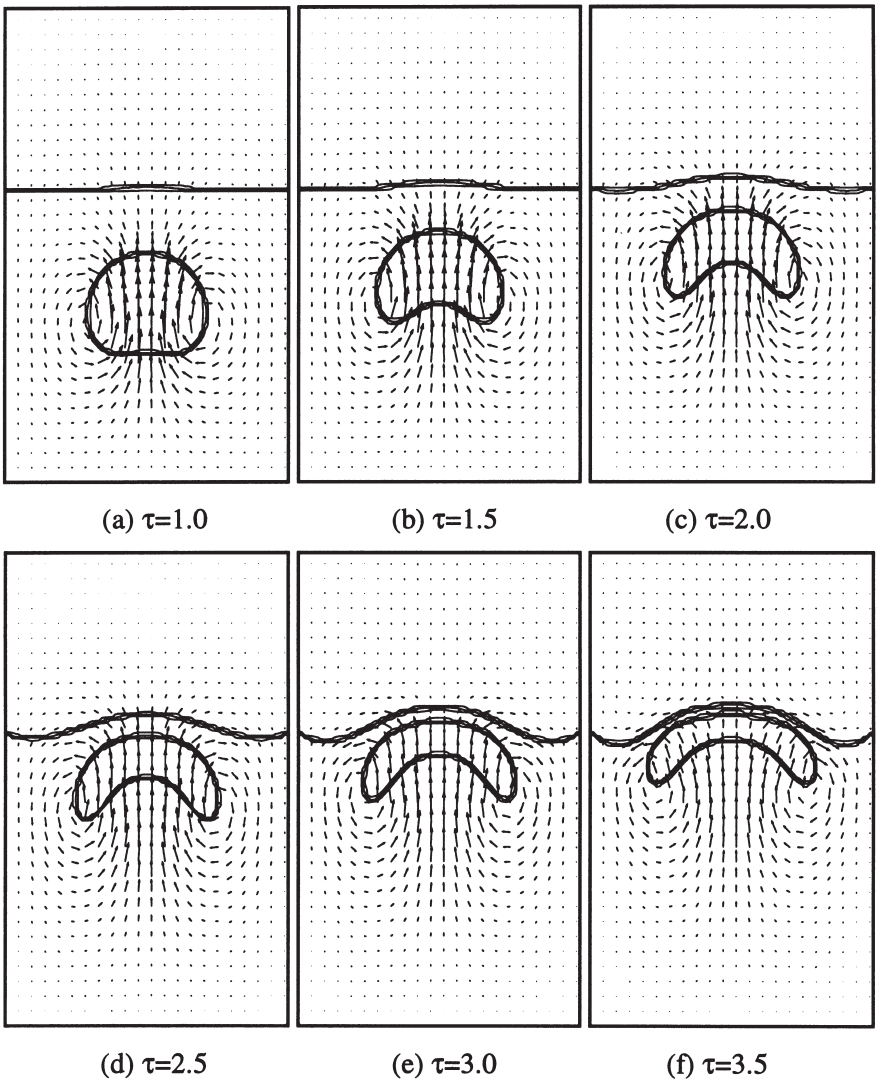

Fig. 11. Velocity field and three contours of F of the values 0.1, 0.5 and 0.9 for a bubble rise towards an interface. (Re = 30, Bo = 10, ρ_f/ρ_g = 100, μ_f/μ_g = 100).

an accurate representation of the interfaces and effective elimination of the numerical diffusion.

6. Conclusion

A robust numerical model for a two-phase fluid system with a high density ratio has been presented. The model accounts for surface tension and adopts high-order convection schemes and a semi-implicit technique. The coalescence of two gas bubbles and the interaction between a bubble and deformable surface in a highly viscous liquid have been simulated. The modified VOF method with the semi-implicit algorithm for solving the velocity field has been shown to be able to represent complex surfaces with reasonable accuracy and its implementation for three-dimensional flows is straightforward. It has been found that complex interfacial phenomena, such as deformation and fragmentation of interfaces, can be well predicted by the present model and a reasonable agreement between numerical simulation and experimental results has been achieved.

Acknowledgements

The code used in this study was developed originally in UNSW under the supervision of Professors J.A. Reizes and E. Leonardi.

References

Brackbill, J.U., Kothe, D.B., Zemach, C., 1992. A continuum method for modeling surface tension. J. Comp. Phys. 100, 335–354.
Chen, L., Garimella, S.V., Reizes, J.A., Leonardi, E., 1996. Analysis of

bubble rise using the VOF method: I. Isolated bubbles. In: ASME Proceedings of the 31st NHT Conference, Houston, 4, 161–173.

Chen, L., Garimella, S.V., Reizes, J.A., Leonardi, E., 1997. Motion of interacting gas bubbles in a viscous liquid including wall effects and evaporation. Num. Heat Transf. Part A 31, 629–654.

Hirt, C.W., Nichols, B.D., 1982. Volume of fluid (VOF) method for the dynamics of free boundaries. J. Comp. Phys. 39, 201–225.

Lafaurie, B., Nardone, C., Scardovelli, R., Zaleski, S., Zanetti, G., 1994. Modelling merging and fragmentation in multiphase flows with SURFER. J. Comp. Phys. 113, 134–147.

Li, Y., 1997. Wavenumber-extended high-order upwind-biased finite-difference schemes for convective scalar transport. J. Comp. Phys. 132, 235–255.

Narayanan, S., Goossens, H.J., Kossen, N.W.F., 1974. Coalescence of two bubbles rising in line at low Reynolds numbers. Chem. Eng. Sci. 29, 2071–2082.

Rider, W.J., Kothe, D.B., Mosso, J., Cerutti, J.H., 1995. Accurate solution algorithms for incompressible multiphase flows, AIAA-95-0699.

Ryskin, G., Leal, L.G., 1984. Numerical solution of free-boundary problems in fluid mechanics—Part 2. Buoyancy-driven motion of a gas bubble through a quiescent liquid. J. Fluid Mech. 148, 19–35.

Unverdi, S.O., Tryggvason, G.A., 1992. Front-tracking method for viscous, incompressible, multi-fluid flows. J. Comp. Phys. 100, 25–37.

Walters, J.K., Davidson, J.F., 1963. The initial motion of a gas bubble formed in an inviscid liquid—Part 2. The three-dimensional bubble and the toroidal bubble. J. Fluid Mech. 17, 321–336.

Youngs, D.L., 1982. Time-dependent multi-material flow with large fluid distortion. In: Morton, K.W., Baines M.J. (Eds.), Numerical Methods for Fluid Dynamics, 273.

Zalesak, S.T., 1979. Fully multi-dimensional flux corrected transport algorithms for fluid flow. J. Comp. Phys. 31, 335–362.